Electronic Research Archive

ERA, 35(1): 164–185.
DOI: 10.3934/era.2027006
Received: 29 June 2026
Revised: 14 October 2026
Accepted: 19 October 2026
Published: 27 November 2026

http://www.aimspress.com/journal/era

Research article

An improved orthogonal subspace exploration method with bilinear factorization for fast matrix completion

Qing Liu*, Lin Ye, Bin Jiang and XianCun Zhou*

School of Electronic Information and Artificial Intelligence, West Anhui University, Lu'an 237012, China.

* **Correspondence:** Email: clyqig2008@126.com, zxc_wx@126.com; Tel: +8615720611026, +8615856428299.

Abstract: Recently, the orthogonal subspace exploration (OSE) method has been introduced for matrix completion, explicitly embedding subspace information to accelerate convergence and improve accuracy. However, because the self-expression matrix in the OSE method inherits both the low-rank property and the full dimension of the original incomplete matrix, it suffers from severe parameter redundancy. This not only restricts further improvement in convergence accuracy but also leads to high computational cost due to required matrix inversion and eigenvalue decomposition. To address these limitations, this paper proposes an improved orthogonal subspace exploration method with bilinear factorization (IOSEBF). The key idea is to impose the orthogonal subspace constraint on a small coefficient matrix obtained via bilinear factorization, rather than on the original high-dimensional incomplete matrix. This strategy significantly reduces both parameter redundancy and computational cost. Experimental results demonstrate that the proposed IOSEBF method is much more accurate than state-of-the-art methods and is hundreds of times faster.

Keywords: low rank; matrix completion; matrix factorization; subspace learning; image processing; QR decomposition

1. Introduction

Low-rank matrix completion is an important technique of recovering the missing information in a partially observed matrix and has received a large amount of interest from researchers in the fields of machine learning [1–5], image processing [6,7], signal processing [8–10], and pattern recognition [11–13]. Since real-world data matrices, such as those for images [14], genetic sequences [15], and traffic flow [16], naturally exhibit a low-rank intrinsic structure, optimizing the rank function of the matrix enables the

recovery of missing information. Because the rank function is discrete and difficult to optimize [17], the nuclear norm (i.e., the summation of singular values of a matrix) is adopted as a replacement in low-rank matrix completion methods, such as the singular value thresholding (SVT) method [18], the approximated proximal gradient search method [19], and the singular value projection method [20]. These methods based on nuclear norm minimization inevitably optimize the nuclear norm, necessitating singular value decomposition (SVD), which leads to high computational complexity and relatively slow speed.

To improve the speeds of nuclear norm minimization methods, some fast completion methods based on matrix factorization have been developed, such as the low-rank matrix fitting method (LMaFit) [21], the fast tri-factorization matrix completion method [22], and the matrix bi-factorization (MBF) method [23]. In these methods, the underlying low-rank matrix is factorized as the product of two or three small submatrices, thereby avoiding the high computational cost of performing SVD on the original large matrix. However, despite their improved efficiency, these methods focus only on the low-rank property of the target matrix and completely ignore other potentially useful features, such as local correlations, side information, and subspace structures inherent in the data. Consequently, they tend to converge slowly and demand many iterations to reach a satisfactory solution. This limitation motivates the incorporation of additional information beyond the pure low-rank assumption.

To address this problem, Yang et al. [24] proposed a feature and nuclear norm minimization method (FNNM) in 2022, which decomposes a matrix into a low-rank global structure and a side-information-driven sparse local pattern. This captures personalized row/column details beyond low-rank assumptions, enabling accurate recovery even with sparse observations and cold-start problems, while improving robustness to noise and outliers. In 2025, Chang et al. [25] introduced an orthogonal complement matrix completion method. Unlike the FNNM method, this method employs orthogonal complement decomposition to handle incomplete side information, achieving a quadratic reduction in sample complexity with respect to side information completeness. Agarwal et al. [26] proposed a robust matrix estimation method with side information in 2026, which decomposes the target matrix into four complementary components. This flexible framework handles both missing-at-random and missing-not-at-random mechanisms, with convergence rates depending on the informativeness of side information. In fact, these methods all leverage external side information to capture local/residual patterns beyond low-rank structures, thereby improving accuracy and robustness under sparse observations.

In contrast to the above side-information-driven methods, the orthogonal subspace exploration (OSE) method proposed by Zhang et al. [27] in 2024 works directly on the observed matrix without any external features. It enforces an orthogonal self-expressive constraint $XV \approx X$ to mine the intrinsic subspace structure of the data itself. The self-expression idea is inspired by subspace clustering [28–31], where each data point is represented as a linear combination of other points to reveal the underlying subspace structure. However, unlike clustering methods, OSE does not aim to produce cluster assignments or centroid updates. It uses the self-expression constraint solely as a structural prior to improve matrix completion. By doing so, OSE remains purely data-driven and avoids the need for potentially unavailable or noisy side information, while still achieving competitive recovery performance through its closed-form optimization. And it has obtained considerable attention from researchers in the fields of pattern recognition [32]. More broadly, subspace modeling has also been explored in other domains. For example, the algebraic state space theory of logical systems provides a matrix-based framework for finite state machines through the semi-tensor product [33]. This cross-disciplinary connection suggests that subspace-based techniques have broad applicability. However, OSE still suffers from several limitations. First, its optimization

requires eigenvalue decomposition and matrix inversion of an $n \times n$ matrix, giving $O(n^3)$ complexity per iteration. Second, it reconstructs the matrix row by row, introducing a nested-loop structure that hurts efficiency. Third, since the self-expression matrix has the same dimensions as X but is inherently low-rank, it carries massive redundancy, which also degrades the convergence accuracy.

To address these limitations, this paper proposes an improved orthogonal subspace exploration method with bilinear factorization (IOSEBF). In the proposed IOSEBF method, the underlying low-rank matrix X is decomposed into the product of two small size submatrices, that is, $X = AB$, where $X \in \mathbb{R}^{m\times n}$, $A \in \mathbb{R}^{m\times r}$ is a column orthogonal matrix, $B \in \mathbb{R}^{r\times n}$ is a coefficient matrix, and $r(0 < r \ll \min(m,n))$ is the estimated rank of X. Then, the main contributions of our proposed IOSEBF method are listed as follows:

- Instead of operating on the original high-dimensional matrix, IOSEBF imposes the orthogonal subspace constraint on a small coefficient matrix B. Consequently, all computationally expensive operations—eigenvalue decomposition, matrix inversion—are reduced from $O(n^3)$ to $O(r^3)$, where $r \ll n$. This significantly accelerates the optimization while preserving the benefits of OSE.
- Our proposed method directly updates the final recovered matrix using QR decomposition and matrix multiplication, eliminating nested loops and obtaining a hundredfold speedup.
- All subproblems in IOSEBF admit closed-form solutions, and the reduced $r \times r$ self-expression matrix lowers parameter redundancy, leading to higher convergence accuracy.

Subspace modeling techniques have been widely explored in various domains. For example, the algebraic state space theory of logical systems provides a matrix-based framework for finite state machines through the semi-tensor product [30]. This cross-disciplinary connection suggests that subspace-based techniques have broad applicability, and the results of this paper are expected to have a certain impact on related research such as matrix completion and subspace learning.

2. Preliminaries

2.1. The SVT method

Since the nuclear norm is the convex envelope of the rank function, it can serve as a surrogate for matrix completion. The SVT method [18] is a representative low-rank matrix completion method based on nuclear norm minimization and has been widely applied. Its optimization model is formulated as:

$$\min_X \|X\|_* + \alpha\|X\|_F^2, \quad s.t. \;\; P_\Omega(X) = P_\Omega(M), \tag{1}$$

where M ($M \in \mathbb{R}^{m\times n}, m \geq n > 0$) is a partially observed matrix with many missing values, X ($X \in \mathbb{R}^{m\times n}$) is the underlying low-rank matrix corresponding to M. α is a non-negative regularization parameter that balances two competing objectives in Eq (1). Ω is the index set of observed entries of M and $P_\Omega(M)$ is the projection operator onto Ω. $\|X\|_*$ is the nuclear norm of X, that is, the summation of singular values of X.

To solve the problem in Eq (1), the SVT method iteratively applies a soft-thresholding operator to the singular values of the current matrix estimate. Let $\tau > 0$ be the thresholding parameter. The SVT operator $\mathcal{D}_\tau(\cdot)$ is defined as the proximal operator of the nuclear norm:

$$\mathcal{D}_\tau(Y) = arg\min_X\{\tau\,\|X\|_* + \tfrac{1}{2}\|X - Y\|_F^2\}, \tag{2}$$

where $Y \in \mathbb{R}^{m\times n}$ is a given real matrix. The closed-form solution of Eq (2) is given as follows:

$$\mathcal{D}_\tau(Y) = U \cdot diag(\max(S-\tau, 0)) \cdot V^T, \tag{3}$$

where $Y = USV^T$ is the SVD decomposition of Y, $U \in \mathbb{R}^{m\times m}$ is the left singular matrix, $V \in \mathbb{R}^{n\times m}$ is the right singular matrix, and $S \in \mathbb{R}^{m\times m}$ is a diagonal matrix whose diagonal entries are the singular values of Y. This operation shrinks small singular values to zero, promoting low-rank solutions while preserving convexity.

SVT benefits from the convexity of the nuclear norm, which ensures global convergence to the optimum of the convex surrogate. However, when applied to real-world images, this solution is often only a local optimum of the original non-convex rank minimization problem, limiting recovery performance. Moreover, each iteration requires a full SVD of an $m \times n$ matrix, incurring $O(n^3)$ complexity that grows rapidly with matrix dimensions.

2.2. The MBF method

To circumvent the high cost of SVD in the SVT method, a fast completion method of MBF [23] has been proposed for matrix completion. In the MBF method, the underlying low-rank matrix X is decomposed as follows:

$$X = AB, \tag{4}$$

where $A \in \mathbb{R}^{m\times r}$ is a column orthogonal normalized matrix, $B \in \mathbb{R}^{r\times n}$ is a coefficient matrix, and r $(0 < r \ll \min(m, n))$ is the estimated rank of X. Then, the minimization model of MBF is formulated as:

$$\min_{A,B,X} \lambda\|B\|_* + \frac{1}{2}\|X - AB\|_F^2,\ s.t. P_\Omega(X) = P_\Omega(M), \tag{5}$$

where λ is a positive regularization parameter. Since the nuclear norm is imposed solely on the smaller $r \times n$ matrix B, SVD is applied to B instead of the full matrix X, which yields a substantial reduction in computational cost.

However, the MBF method has notable drawbacks. It depends exclusively on the low-rank assumption and the nuclear norm surrogate, neglecting other useful structures, such as subspace geometry and local correlations. This over-simplification leads to slow convergence and a high number of iterations, especially under sparse observations or noisy conditions, where additional structural priors are essential for accurate recovery.

2.3. The OSE method for matrix completion

In 2024, Zhang et al. [27] proposed an OSE matrix completion method. It is a purely data-driven method that mines the intrinsic subspace structure directly from the observed matrix, enforces an orthogonal self-expressive constraint, and is formulated as:

$$\begin{gathered}\min_{X,V,\Lambda} \|XV - X\|_F^2 + \lambda tr(X\Lambda X^T) + 2\mu tr(V) \\ s.t. P_\Omega(X) = P_\Omega(M), tr(\Lambda^+) = 1, \Lambda \geq 0, V^T V = I_n\end{gathered}, \tag{6}$$

where $V \in \mathbb{R}^{n\times n}$ is an orthogonal self-expression matrix, $\Lambda \in \mathbb{R}^{n\times n}$ is a positive semi-definite diagonal matrix, Λ^+ the Moore–Penrose inverse of Λ, $tr(V)$ is the trace function of V, and I_n denotes the

$n \times n$ identity matrix. $\mu > 0$ prevents the trivial solution $V = I_n$ via the trace penalty $tr(V)$. $\lambda > 0$ is a regularization parameter controlling the contribution of the surrogate $tr(X\Lambda X^T)$.

The optimization model in Eq (6) can be effectively solved via an alternating minimization method, a popular strategy for handling multi-block convex or nonconvex problems. In this method, each variable block is optimized sequentially while the remaining blocks are held fixed. A key advantage of the proposed formulation is that, with the remaining variables fixed, the subproblem associated with each variable block becomes convex. Consequently, it allows us to obtain a closed-form solution for each subproblem, thereby avoiding the need for inner iterative solvers or approximate updates.

First, by fixing the variables X and V, the variable Λ is updated by solving the subproblem as follows:

$$\min_{\Lambda} tr(X\Lambda X^T),\ s.t.\ tr(\Lambda^+) = 1, \Lambda \geq 0, \tag{7}$$

which yields the closed form solution,

$$\Lambda = \left(\frac{(X^TX)^{1/2}}{tr((X^TX)^{1/2})}\right)^+. \tag{8}$$

Second, by fixing X and Λ, the variable V is updated by solving the following subproblem:

$$\min_{V} \|XV - X\|_F^2 + 2\mu tr(V). \tag{9}$$

The minimization problem in Eq (9) is equivalent to maximizing $tr(V^T(X^TX - \mu I))$, and its closed-form solution is shown as follows:

$$V = U_r U_l^T, \tag{10}$$

where U_l and U_r are the left singular matrix and right singular matrix of $X^TX - \mu I$, respectively. This step requires an SVD or eigenvalue decomposition of an $n \times n$ matrix, which costs $O(n^3)$ and becomes the main computational bottleneck for large matrices.

Finally, the recovery result X is updated by solving the following subproblem:

$$\min_{X} tr(XWX^T), \quad s.t.\ P_\Omega(X) = P_\Omega(M), \tag{11}$$

where $W = (V - I)(V - I)^T + \lambda\Lambda$. This convex quadratic problem decouples across rows. For each row i, let I_i be the set of observed columns. The optimal solution is obtained row-wise as:

$$x^i = \widehat{m}^i (P_i W^{h_i +} P_i)^{p_i +} (H_i W H_i)^{p_i +}, \tag{12}$$

where P_i is the diagonal projection matrix for the observed entries, H_i indicates nonzero diagonal entries of Λ, and $p_i = diag(P_i)$. This closed-form update is derived from the KKT conditions, avoiding iterative optimization. However, this row-wise update can exploit local information but introduces nested loops and may overfit local patterns, leading to premature convergence to a local optimum.

The main steps of the OSE method for updating the variables, that is, Λ, V, and X, are summarized in Algorithm 1.

From the updating steps in Algorithm 1, all subproblems of OSE admit closed-form solutions: Λ via matrix square root, V via eigenvalue decomposition to compute the left and right singular matrices, and X row-wise via linear systems. Consequently, the algorithm requires no step-size tuning and is easy to implement. Moreover, despite the non-convex surrogate, OSE is theoretically guaranteed to converge to a global optimum. Empirically, it converges within dozens of iterations, which is significantly faster than

many factorization-based methods that often need hundreds or thousands of iterations. Thus, OSE is both efficient and robust in practice.

Algorithm 1. The main steps of OSE.

Input: M is an incomplete matrix; $\lambda > 0, \mu > 0$.
Repeat:
Update Λ by Eq (8);
Update V by Eq (10);
Update X by Eq (12);
Until: convergence.
Output: X is the recovered matrix.

However, OSE also has some notable drawbacks. First, its per-iteration cost is dominated by eigenvalue decomposition and matrix inversion of an $n \times n$ matrix, leading to $O(n^3)$ complexity, which becomes prohibitive for large-scale problems. Second, row-wise reconstruction of X introduces nested loops, which hinders vectorized operations and fine-grained parallelism. This becomes a major bottleneck under large scale cases. Third, the convergence accuracy of OSE may be limited because its self-expression matrix V is of size $n \times n$, which is much larger than the true rank of X, resulting in severe parameter redundancy.

3. Our proposed method

3.1. The minimization model of IOSEBF

To preserve the advantages of OSE, namely being purely data driven, having closed-form updates, and converging rapidly, while improving its speed and convergence accuracy, we propose an IOSEBF.

The key idea is first to factorize the underlying low-rank matrix X into the product of two small sub-matrices, that is, A and B, as shown in Eq (4). Then, the orthogonal subspace constraint is imposed on the coefficient matrix B rather than on X. This reduces expensive operations to a low-dimensional subspace ($r \ll n$), dramatically improving scalability while preserving the data-driven, closed-form nature of OSE. The IOSEBF minimization model is shown as follows:

$$\begin{aligned} &\min_{A,B,X,\bar{V}} \|B^T\bar{V} - B^T\|_F^2 + \lambda\|X - AB\|_F^2 + \mu tr(\bar{V}) \\ &s.t. \quad P_\Omega(X) = P_\Omega(M),\ \bar{V}^T\bar{V} = I_r \end{aligned}, \tag{13}$$

where I_r denotes the $r \times r$ identity matrix. The parameter $\lambda > 0$ balances the fitting term, and the parameter $\mu > 0$ prevents the trivial solution $\bar{V} = I_r$. $\bar{V}$ is an orthogonal self-expression matrix in size of $r \times r$ ($r \ll \min(m, n)$)**.** The proposed model in Eq (13) contains three key designs, whose respective roles are described as follows.

- The bilinear factorization module. The factorization $X = AB$ replaces the full-size X with $A \in \mathbb{R}^{m\times r}$ and $B \in \mathbb{R}^{r\times n}$. It avoids full SVD, reduces computational complexity, and preserves the low-rank structure. More importantly, it reduces all subsequent subspace operations to a low-dimensional space, which is the basis for the efficiency gain over OSE.

- The low-dimensional orthogonal self-expression term. The term $\|B^T\bar{V} - B^T\|_F^2$ performs subspace learning on the row space of B, encouraging its rows to lie in a low-dimensional subspace captured by $\bar{V}$. Since B projects the column-orthogonal basis A back to the original space, this term indirectly regularizes X. MBF and IOSEBF both adopt the same bilinear factorization and the same reduced dimension r. Their difference lies in that MBF uses the nuclear norm to promote low-rankness, whereas IOSEBF replaces it with explicit subspace learning on the row space of B. This term enables IOSEBF to exploit the latent subspace structure of the data in addition to the low-rank property. Compared with OSE, IOSEBF uses an $r \times r$ subspace variable $\bar{V}$ instead of the $n \times n$ variable V. Hence, it reduces the number of subspace parameters from $O(n^2)$ to $O(r^2)$. In this way, IOSEBF alleviates the parameter redundancy problem of OSE while preserving the subspace learning capability inherited from OSE.
- The trace penalty and orthogonal constraint. The trace penalty $\mu tr(\bar{V})$ prevents the trivial solution $\bar{V} = I_r$, which would otherwise make the self-expression term vanish and extract no meaningful subspace. If $\mu = 0$, the model degenerates to LMaFit [21], retaining only the bilinear factorization term. Thus, the trace penalty is essential. Moreover, unlike the $n \times n$ matrix V in OSE, $\bar{V}$ is only $r \times r$. This reduces computation and parameter redundancy, making $\bar{V}$ easier to optimize.

3.2. The optimization of IOSEBF

The optimization model of our proposed IOSEBF method can be solved via an alternating minimization method, that is, the variables in Eq (13) can be updated one by one with the rest fixed.

First, the self-expression matrix $\bar{V}$ can be updated by solving the following sub-problem,

$$\min_{\bar{V}} \|B^T\bar{V} - B^T\|_F^2 + \mu tr(\bar{V}), \tag{14}$$

where the variable B has been fixed. The problem in Eq (14) is equal to the minimization problem as follows:

$$\max_{\bar{V}} tr(\bar{V}^T C), \tag{15}$$

where $C = BB^T - \mu I_r$ and I_r is an identity matrix. It is clear to see that the closed-form solution of the optimization problem in Eq (15) is that

$$\bar{V} = U(sign(S))U^T, \tag{16}$$

where $C = USU^T$ is the eigenvalue decomposition of C. Since $\bar{V}$ is only $r \times r$, this step brings two benefits compared with OSE.

- It reduces the eigenvalue decomposition cost and accelerates IOSEBF. As shown in Eq (10), OSE requires an eigenvalue decomposition of an $n \times n$ matrix, costing $O(n^3)$. In IOSEBF, the corresponding matrix is only $r \times r$, so the cost is $O(r^3)$. Since $r \ll n$, this substantially reduces the per-iteration cost.
- It alleviates the parameter redundancy of the OSE subspace matrix. To facilitate understanding, we assume the ground-truth rank of X is $r_1 (0 < r_1 \ll \min(m, n))$. In OSE, although the underlying low-rank matrix X has rank $r_1 \ll n$, the self-expression matrix V is still of size $n \times n$. The extra $n^2 - {r_1}^2$ degrees of freedom do not correspond to the true low-rank structure

and may absorb noise, which increases the risk of overfitting and degrades the recovery accuracy. In contrast, the subspace variable $\bar{V}$ in IOSEBF has only r^2 parameters, and its dimension is much closer to the true rank r_1 than the $n \times n$ matrix in OSE. This reduction in parameter redundancy restricts the optimization to a smaller and better-conditioned space and thus improves the generalization accuracy.

Second, the matrix A is updated by fixing B and X. In our Eq (13), A appears only in the term of $\|X - AB\|_F^2$. Therefore, the matrix A is optimal solution to the following sub-problem, that is,

$$\min_A \|X - AB\|_F^2. \tag{17}$$

In fact, minimizing the problem in Eq (17) is equivalent to,

$$\min_A \|A - XB^T\|_F^2. \tag{18}$$

Because the matrix A is column-orthogonal, we can compute a QR decomposition of XB^T to obtain an orthonormal basis:

$$A = qr(XB^T, 'eco'), \tag{19}$$

where $qr(XB^T, 'eco')$ stands for extracting the orthogonal basis of XB^T by using an economy-size (thin) QR decomposition. The thin QR decomposition in Eq (19) costs only $O(mr^2)$ operations and can be efficiently parallelized using standard linear algebra libraries, yielding a fast, scalable update for A while avoiding the nested loops of the original OSE.

Third, the coefficient matrix B is set to the optimal solution of the problem as follows:

$$\begin{aligned} B &= arg \min_B \|B^T\bar{V} - B^T\|_F^2 + \lambda\|X - AB\|_F^2 \\ &= arg \min_B \|\bar{V}^T B - B\|_F^2 + \lambda\|B - A^T X\|_F^2, \end{aligned} \tag{20}$$

where the matrices $\bar{V}$, A, and X have been fixed. Setting the derivative to zero yields,

$$QB = \lambda A^T X, \tag{21}$$

where $Q = (I - \bar{V})(I - \bar{V})^T + \lambda I_r$. Therefore, we have

$$B = \lambda Q^{-1} A^T X, \tag{22}$$

with Q^{-1} being the inverse of Q. Since Q is of size $r \times r$ with $r \ll n$, its inversion costs only $O(r^3)$, which is negligible compared to the $O(n^3)$ operations in OSE. Hence, the update of B is far more efficient.

Then, the variable $\bar{V}$ acts as a hard-thresholding subspace filter that improves anti-noise ability. From Eq (16), $\bar{V}$ is a symmetric orthogonal matrix with eigenvalues ±1. Its +1 eigenspace corresponds to the dominant directions of B, that is, directions where the eigenvalues of BB^T are larger than μ; its −1 eigenspace corresponds to small-energy directions, which are typically noise-dominated. On the +1 eigenspace, Q has eigenvalue λ, while on the −1 eigenspace, Q has eigenvalue $4 + \lambda$. Since $B = \lambda Q^{-1} A^T X$ by Eq (22), the effective coefficient on the +1 eigenspace is 1, whereas that on the −1 eigenspace is $\frac{\lambda}{4+\lambda} < 1$. Thus, the update of B preserves and enhances the dominant subspace while suppressing the noise-dominated subspace. Therefore, $\bar{V}$ acts as a hard-thresholding subspace filter.

Finally, the recovered matrix of the optimization model shown in Eq (13) is updated as follows:

$$X = AB + P_\Omega(M) - P_\Omega(AB). \tag{23}$$

This step ensures that X satisfies the observed entries exactly while inheriting the low-rank structure from AB. In contrast, OSE updates X row by row (Eq (12)) by solving a linear system for each observed row, which creates nested loops that hinder vectorization and parallelization. The proposed IOSEBF method extracts the global feature basis A via QR decomposition, obtains B through the low-dimensional subspace variable $\bar{V}$, and forms $X = AB$. Hence, it is fully vectorized and better exploits the global structure, avoiding the overfitting issue of the row-wise update in OSE. Thus, IOSEBF eliminates the row-wise bottleneck of OSE and achieves much higher accuracy than OSE. The main steps of our proposed IOSEBF method are summarized in Algorithm 2.

Algorithm 2. The main steps of IOSEBF.

Input: M is an incomplete matrix; $\lambda > 0, \mu > 0$.
$r > 0$ is the estimated rank of X.
Repeat:
Update $\bar{V}$ by Eq (16);
Update A by Eq (19);
Update B by Eq (22);
Update X by Eq (23);
Until: convergence.
Output: X is the recovered matrix.

Thus, IOSEBF retains the data-driven, closed-form nature of OSE while achieving substantially higher computational efficiency and better convergence accuracy.

3.3. The Computation complexity of IOSEBF

In this section, we compare the per-iteration computational complexity of the proposed IOSEBF method with that of the original OSE method. For simplicity, we assume the matrix to be square, that is, $m = n$. This assumption is suitable because the performance of both methods is dominated by the larger dimension when $m \neq n$, and setting $m = n$ allows us to focus on the essential difference in complexity. Table 1 summarizes the dominant operations and the corresponding asymptotic complexities for each variable in one iteration of OSE and IOSEBF.

Table 1. Per-iteration computational complexity of OSE and IOSEBF (general dense case).

Variable	OSE	IOSEBF
$V/\bar{V}$	$O(n^3)$	$O(r^3)$
A	×	$O(nr^2)$
B	×	$O(nr^2)$
X	$O(n^3)$	$O(nr^2)$
Total complexity	$O(2n^3)$	$O(3nr^2 + r^3)$

As shown in Table 1, the original OSE method requires $O(n^3)$ operations for updating both V and X. Consequently, its total per-iteration complexity is $O(2n^3)$. In contrast, the proposed IOSEBF method updates $\bar{V}$ with only $O(r^3)$ operations, while the updates of A, B, and X are all bounded by

$O(nr^2)$with $r \ll n$. Therefore, the total per-iteration complexity of IOSEBF is $O(3nr^2 + r^3)$. Since the rank r is much smaller than n, the IOSEBF method achieves a dramatic reduction in computational cost compared to OSE. This advantage makes IOSEBF highly suitable for large-scale matrix completion tasks.

3.4. The convergence analysis of IOSEBF

Suppose $\{A_k, B_k, X_k, \bar{V}_k\}$ is the sequence generated by IOSEBF, and $F_k = F(A_k, B_k, X_k, \bar{V}_k)$ is the objective function value of our proposed IOSEBF at its kth iteration, where $k \geq 1$ and the objective function has been defined in Eq (13). It is easy to see that

$$F_k >= F_{k+1}, \tag{24}$$

that is, the objective function is non-increasing, because each subproblem of IOSEBF is convex and solved exactly to global optimality.

Theorem I. The sequence $\{X_k\}$ given by IOSEBF will converge, that is,

$$\lim_{k \to +\infty} \|X_k - X_{k+1}\|_F = 0, \tag{25}$$

where $k \geq 1$.

Proof. In thek^{th} iteration of IOSEBF, after updating $A_k, B_k,$ and $\bar{V}_k$, the matrix $X_{k+1}$is updated by solving the subproblem,

$$X_{k+1} = arg \min_X \phi(X), \tag{26}$$

where $\phi(X) = \lambda\|X - C_{k+1}\|_F^2$ and $C_{k+1} = A_{k+1}B_{k+1}$. Because $\phi(X)$ is strongly convex with $\lambda > 0$, the following inequality holds,

$$\phi(X_k) \geq \phi(X_{k+1}) + \lambda\|X_k - X_{k+1}\|_F^2. \tag{27}$$

Then, we have that

$$\phi(X_{k+1}) \leq \phi(X_k) - \lambda\|X_k - X_{k+1}\|_F^2. \tag{28}$$

Since the other terms in the objective function $F(\cdot)$ are unchanged during this step, it is easy to have,

$$F_{k+1} \leq F(A_{k+1}, B_{k+1}, X_k, \bar{V}_{k+1}) - \lambda\|X_k - X_{k+1}\|_F^2, \tag{29}$$

Since the updates of $\bar{V}$, A, and B also decrease the objective, we have the following conclusion,

$$F_{k+1} \leq F_k - \lambda\|X_k - X_{k+1}\|_F^2. \tag{30}$$

According to Eq (30), we obtain,

$$F_k - F_{k+1} \geq \lambda\|X_k - X_{k+1}\|_F^2. \tag{31}$$

By summing both sides of the inequality in Eq (31) for $k = 1$ to n, it is easy to have,

$$\lambda \sum_{k=1}^{n} \|X_k - X_{k+1}\|_F^2 \leq F_1 - F_{n+1}. \tag{32}$$

According to the model in Eq (13), it is not difficult to have,

$$F_{n+1} \geq -\mu r. \tag{33}$$

In view of Eqs (32) and (33), the following conclusion is obtained,

$$\lambda \sum_{k=1}^{n} \|X_k - X_{k+1}\|_F^2 \leq F_1 + \mu r. \tag{34}$$

Then, we have,

$$\lim_{k \to +\infty} \|X_k - X_{k+1}\|_F = 0. \tag{35}$$

That concludes the proof.

4. Experimental result

In this section, we evaluate the proposed IOSEBF method on synthetic data and several real-world images containing many randomly missing entries. The performance of IOSEBF is compared against several state-of-the-art matrix completion methods in terms of both convergence accuracy and computational speed. These competing methods are listed as follows:

- AROMC [5]: Adaptive rank-one matrix completion using sum of outer products
- MBF [23]: Matrix bi-factorization via alternating minimization for low-rank recovery and completion
- FNNM [24]: Feature and nuclear norm minimization for matrix completion
- OSE [27]: Orthogonal subspace exploration for efficient matrix completion
- HOAT [34]: Half-quadratic optimization based on adaptive truncated-quadratic loss function

All experiments are conducted in the MATLAB R2019a environment on a laptop equipped with an Intel Core i9 processor and 32 GB of RAM to ensure a fair and reproducible comparison. All the parameters for the compared methods have been tuned to be optimal. The code for IOSEBF is available online at https://github.com/LQNY/IOSEBF.

4.1. *Matrix completion on synthetic data*

In this section, the proposed IOSEBF method is tested on synthetic data matrix with predefined rank. The synthetic matrix is generated as follows:

$$D = D_L D_R + \sigma \cdot P_\Omega(rand(m,n)), \tag{36}$$

where $D_L = random(m, r_1)$ is a random matrix, $D_R = random(r_1, n)$, and $1 \leq r_1 \ll min(m,n)$ is the true rank of D. The parameter $\sigma \geq 0$ controls the noise level, that is, the recoverability of matrix D degrades as σ increases. In this section, we let $m = n = 200$ and the true rank $r_1 = 20$ for generating the tested matrix D. There're 50% of entry values are randomly selected and replaced with zero to generate incomplete matrix.

First, the effect of parameter r, that is, the estimated rank of D, is tested to guide parameter setting for the proposed IOSEBF method. By letting the parameter r increase from 1 to $m \times 40\%$, with a step size equal to 2, the IOSEBF method is tested by using the synthetic matrix generated as in Eq (36) and its convergence accuracy is compared with that of the MBF method.

The normalized Frobenius error (NFE) of recovery result is chosen as the evaluation criterion for IOSEBF and it is defined as follows:

$$NFE = \frac{\|X_{ori} - X_{rec}\|_F}{m \times n}, \tag{37}$$

where X_{ori} is the original matrix and X_{rec} is a recovered matrix. The curves of NFE versus r of IOSEBF and MBF are plotted in Figure 1.

From Figure 1, it is evident that the proposed IOSEBF method is significantly more robust to the parameter r than the MBF method. The NFE of MBF decreases sharply as r increases from 1 to 21, reaching its minimum at $r = 21$, and then increases smoothly for $r > 21$. This behavior indicates that MBF is highly sensitive to the choice of r: when r is smaller than the true rank of D, the model is under-parameterized and cannot accurately recover the incomplete matrix $P_\Omega(D)$; when r exceeds the true rank, over-parameterization leads to increased reconstruction error, likely due to overfitting or numerical instability. In contrast, the IOSEBF method maintains a consistently low NFE across the entire tested range of r, with only mild fluctuations. This demonstrates that IOSEBF does not require precise tuning of $r$and can automatically adapt to the underlying rank of the data. As a result, IOSEBF offers two key advantages over MBF: (1) higher accuracy over a wide range of r and (2) superior practical usability because it eliminates the need for exhaustive parameter selection. Therefore, IOSEBF is a more reliable and efficient matrix completion method, especially in real-world scenarios where the true rank is unknown.

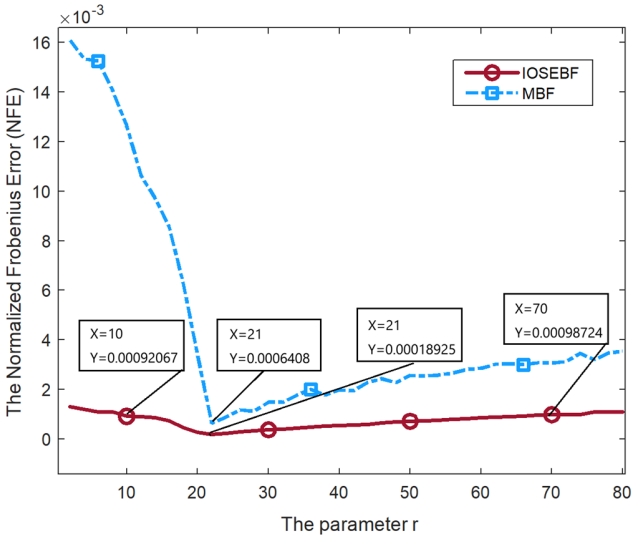

Figure 1. The effect of r on IOSEBF. The size of D is 200 × 200, the true rank is 20 and the noise level σ = 0. IOSEBF is tested with λ fixed at 100 and μ at 6000, while r ranges from 1 to 80.

Second, the effects of λ and μ on IOSEBF are then tested separately by fixing the other parameter, with r held constant, that is, $r = 30$. The NFE curves of IOSEBF versus λ and μ are shown in Figures 2 and 3 (the latter on the next page), respectively.

Figure 2 demonstrates that there're two key characteristics of the IOSEBF method with respect to the parameter λ. First, as λ increases from 10 to 200, the NFE decreases monotonically and reaches its minimum at $\lambda = 200$, indicating that moderate regularization improves reconstruction accuracy by mitigating overfitting. Second, and more importantly, for a wide range of λ from 50 to 300, the NFE of IOSEBF remains consistently smaller than 5×10^{-4}, which is significantly better than the best NFE achieved by MBF at its optimal parameter $r = 21$ in Figure 1. This clearly shows that IOSEBF is

insensitive to the choice of λ and does not require delicate tuning. Therefore, IOSEBF offers both high accuracy and ease of use, making it particularly suitable for practical applications.

The curve in Figure 3 shows that the IOSEBF method exhibits strong robustness to the parameter μ. Specifically, when μ is as small as 1000, the NFE is relatively high, indicating a poor recovery. However, once μ reaches 1500, the NFE drops sharply to approximately 4.0×10^{-4} and remains almost unchanged across a wide range of μ values (e.g., from 1500 to 6000), with only negligible fluctuations between 4.0×10^{-4} and 4.2×10^{-4}. This flat response clearly demonstrates that beyond a moderate threshold, the performance of IOSEBF becomes insensitive to the exact choice of μ. Therefore, the strong robustness of IOSEBF to μ not only simplifies parameter selection in practice but also guarantees consistently high reconstruction accuracy even when μ is not finely optimize

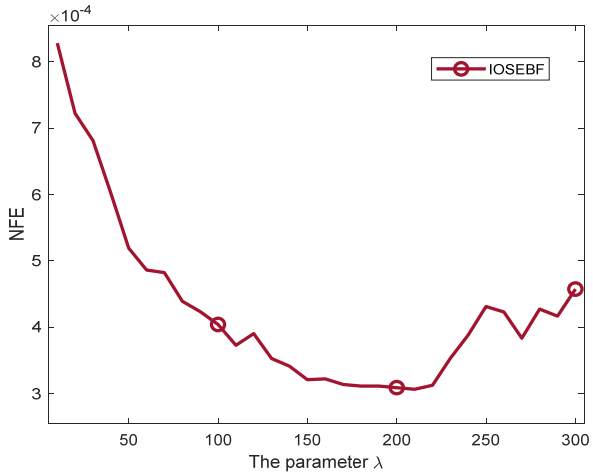

Figure 2. The effect of λ on IOSEBF with r = 30 and μ = 6000. IOSEBF is tested by letting the parameter λ increase from 10 to 300 with a step size equal to 10.

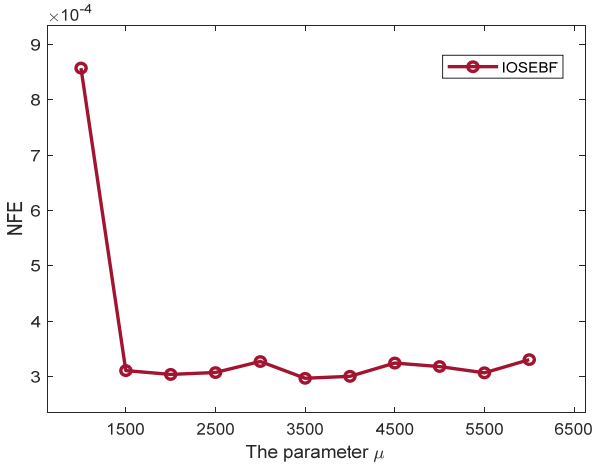

Figure 3. The effect of μ on IOSEBF with r = 30 and λ = 200. IOSEBF is tested by letting the parameter μ increase from 100 to 6000 with a step size equal to 500.

Finally, the robustness of IOSEBF to the noise level is evaluated on synthetic data from Eq (36) of size 1000×1000 by varying σ from 0.1 to 0.9 in increments of 0.1. The NFE values of our proposed IOSEBF method and other compared methods, that is, AROMC, FNNM, HOAT, and OSE, are listed in Table 2.

Table 2. The NFE values of IOSEBF and other compared methods on synthetic data with different noise level. The maximum iteration numbers for IOSEBF, OSE, MBF, HOAT, AROMC, and FNNM are equal to 100, 100, 100, 50, 100, and 200, respectively.

Noise level (σ)	FNNM	AROMC	HOAT	MBF	OSE	IOSEBF
0.1	2.66e-04	5.85e-04	7.23e-05	9.94e-05	**7.15e-05**	8.09e-05
0.2	2.95e-04	5.88e-04	1.34e-04	1.69e-04	1.26e-04	**1.11e-04**
0.3	3.14e-04	6.03e-04	1.86e-04	2.46e-04	1.82e-04	**1.61e-04**
0.4	3.36e-04	6.17e-04	2.49e-04	3.29e-04	2.36e-04	**2.12e-04**
0.5	3.55e-04	6.34e-04	2.81e-04	4.09e-04	2.91e-04	**2.61e-04**
0.6	3.78e-04	6.56e-04	3.44e-04	4.92e-04	3.49e-04	**3.13e-04**
0.7	3.99e-04	6.79e-04	3.97e-04	5.74e-04	4.01e-04	**3.65e-04**
0.8	4.21e-04	7.08e-04	4.39e-04	6.53e-04	4.56e-04	**4.17e-04**
0.9	4.69e-04	7.37e-04	4.72e-04	7.37e-04	5.11e-04	**4.63e-04**

Table 2 reports the NFE values of IOSEBF and other compared methods under increasing noise levels ($\sigma = 0.1$ to 0.9) on synthetic data. Overall, the proposed IOSEBF method achieves the most competitive performance, especially at moderate and high noise levels. For $\sigma = 0.1$, the HOAT and OSE methods converge more accurately than our proposed IOSEBF method does. However, for $\sigma \geq 0.2$, the IOSEBF method consistently outperforms the HOAT, FNNM, AROMC, and MBF methods. The main reason is that the IOSEBF method can obtain the intrinsic subspace structure of the incomplete matrix by optimizing a self-expression matrix. Among all methods, the AROMC method gives the highest NFE across all noise levels, indicating the weakest robustness. The MBF and FNNM methods also show considerably larger errors than IOSEBF, with the gap widening as noise increases. The closest competitor is OSE: at low noise level, that is, $\sigma = 0.1$ and 0.2, their performance is comparable, but from $\sigma = 0.3$ onward IOSEBF maintains a clear advantage. Overall, IOSEBF exhibits superior accuracy and noise robustness, attaining the lowest average NFE among all six methods, and is therefore recommended for synthetic data restoration tasks.

IOSEBF surpasses the original OSE method not only in convergence accuracy but, more notably, in speed. The CPU times of the IOSEBF and other compared methods are plotted in Figure 4.

Figure 4 shows that the IOSEBF method is the fastest matrix completion method, while the OSE method is the slowest one among the six tested methods. The actual CPU time of OSE fluctuates between 150 s and 280 s, consuming much more time than the other methods. The main reason is that OSE requires computing the inverse of the original matrix to be recovered at each iteration, and the program contains a double-loop structure. The method slightly faster than OSE is HOAT, with a total time consumption of about 150 s. Similar to OSE, the HOAT method also needs to recover the reconstructed result matrix row by row and column by column, resulting in a high total computational cost. When the noise level is less than 0.4, the CPU time of AROMC is close to that of HOAT. And

when the noise level is greater than 0.4, its CPU time is close to that of FNNM. This phenomenon indicates that when the noise level is high, the AROMC method prematurely converges to a local optimum and stops searching for a better solution. The complexity of the FNNM method is basically the same as that of HOAT and OSE, but its CPU time is significantly smaller. The important reason is that the number of iterations of the FNNM method is smaller. The CPU time of the MBF method fluctuates between 1.2 s and 4.2 s, indicating that its number of iterations changes significantly with the noise level. Nevertheless, the CPU time of MBF is still significantly smaller than that of OSE and other methods, mainly because MBF performs SVD decomposition only on submatrices of small dimensions, thereby reducing the total computational cost.

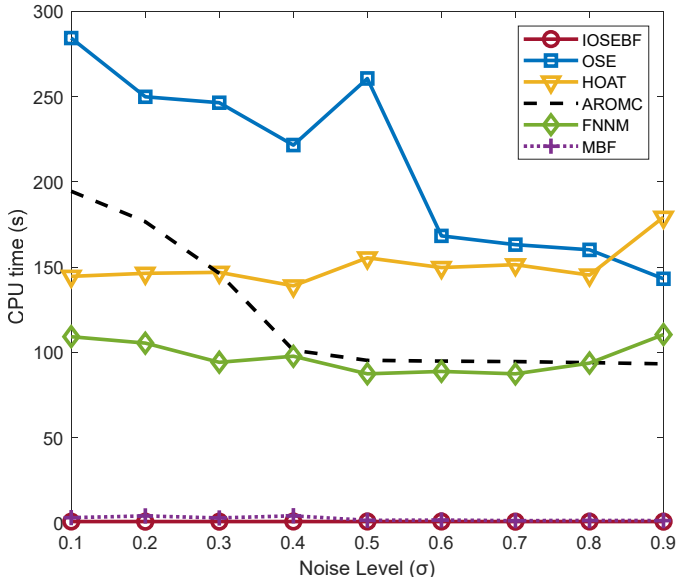

Figure 4. CPU time of IOSEBF and the other five compared methods. The noise level of the tested incomplete matrices increases from 0.1 to 0.9 with a step size of 0.1.

The IOSEBF method is the fastest, with its CPU time fluctuating between 0.7 s and 0.9 s, completing all tasks almost very stably. Although the speed of the MBF method is relatively close to that of IOSEBF, the convergence accuracy of the latter is much higher than that of the former. Therefore, our proposed IOSEBF method performs much better than the OSE method does in terms of both CPU time and convergence accuracy.

4.2. Matrix completion on real world images with random missing values

In this section, the proposed IOSEBF method is evaluated on several real-world color images of size 1024×1024, which are shown in Figure 5.

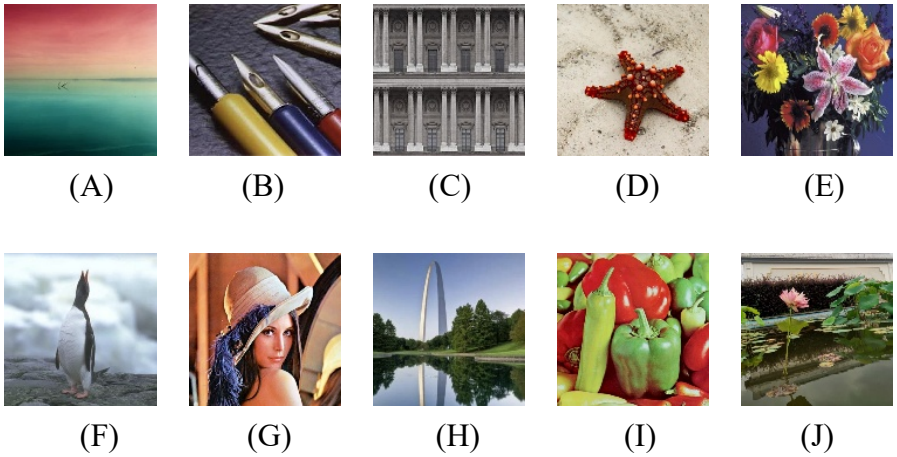

Figure 5. The original color images used for matrix completion. Each image is of size 1024×1024 pixels.

The peak signal-to-noise ratio (PSNR) is selected as a measurement of convergence accuracy for the IOSEBF method and is formulated as follows:

$$PSNR = 10 \cdot log_{10} \frac{255^2}{MSE}, \tag{38}$$

where MSE is defined as follows:

$$MSE = \frac{1}{3T \cdot SE}, \tag{39}$$

where T is the total number of entries of the incomplete matrix and SE is formulated as follows:

$$SE = \sum_{i=1}^{3} ERR_i, \tag{40}$$

$$ERR_i = \left\| X_i - \hat{X}_i \right\|_F^2, \tag{41}$$

where X_i is the ith channel of the original matrix X and $\hat{X}_i$ is the ith channel of the recovery result given by a matrix completion method. Since the original color image has three channels, that is, R, G, and B, each channel is recovered independently.

The incomplete images are generated by randomly selecting 50% of the entries in the original color images plotted in Figure 5 and marking them as missing. Using these incomplete images, IOSEBF is tested, and its convergence accuracy and CPU time are compared with those of the OSE, HOAT, AROMC, FNNM, and MBF methods. For IOSEBF, the parameter λ is set to 120, and μ is initialized at 100 and multiplied by 1.01 at each iteration. The rank r is selected by a lightweight rank-selection strategy over a small candidate set {35, 55, 75, 95, 115}, where each candidate is run for only 100 iterations and the one with the smallest relative error on the observed entries is chosen. The PSNR values of IOSEBF and other compared methods are listed in Table 3.

The results in Table 3 shows that the PSNR values of the MBF method are the lowest among all tested algorithms because it does not take into account external matrix feature information nor the internal subspace information of the matrix. Due to the fact that the FNNM method fully considers the row and column feature information of the incomplete matrix to be recovered, it achieves PSNR values

significantly better than those of the MBF method. The PSNR values of AROMC are much better than those of MBF and FNNM under most cases, the main reason is that it can dynamically adjust the rank of the matrix according to the image content, thereby avoiding the bias caused by manually setting the rank parameter. The HOAT method achieves good results on certain images, that is, images (B), (F), and (I), while it suffers from poor robustness and high sensitivity to variations in image content, which limits its suitability as a general-purpose solution. For applications that demand high accuracy and stability, the HOAT method is inferior to both AROMC and IOSEBF.

Table 3. The PSNR values of IOSEBF and other five methods. The missing ratio of each color incomplete image is 50%. The maximum iteration numbers for IOSEBF, OSE, MBF, HOAT, AROMC, and FNNM are equal to 100, 100, 200, 50, 150, and 300, respectively.

Image index	FNNM	AROMC	HOAT	MBF	OSE	IOSEBF
(A)	47.49	49.31	49.14	46.28	49.12	**49.74**
(B)	38.51	37.71	39.66	35.64	39.53	**40.32**
(C)	37.54	38.71	38.43	36.52	38.46	**39.61**
(D)	32.01	31.86	31.48	32.65	33.56	**34.15**
(E)	33.87	33.45	33.58	32.26	34.67	**36.17**
(F)	39.62	40.41	40.32	35.09	40.52	**41.99**
(G)	32.54	32.38	32.23	29.06	33.63	**35.26**
(H)	37.95	39.32	38.78	37.49	38.81	**40.82**
(I)	40.12	42.34	42.38	40.37	42.64	**43.61**
(J)	32.18	31.77	31.30	29.66	32.95	**33.93**

Table 3 also shows that OSE consistently outperforms MBF, FNNM, and HOAT in terms of PSNR across the ten test images and achieves comparable or better performance than AROMC in most cases, with particularly clear advantages on images D, G, and E. Two fundamental characteristics account for this superior performance. On the one hand, OSE imposes an orthonormal constraint on the self-representation matrix, which forces the learned subspace to be orthogonal. This design enables the algorithm to exploit the linear relationships among rows and columns, a property completely overlooked by the MBF, FNNM, AROMC, and HOAT methods, because they rely solely on global low-rank assumptions without considering local correlations. On the other hand, OSE adopts a differentiable non-convex objective function that allows each variable to be updated via closed-form expressions. As a result, the method does not require manual tuning of step sizes, which is a common burden for gradient-based optimizers, nor does it suffer from the slow convergence often exhibited by AROMC and HOAT.

As reported in Table 3, IOSEBF achieves the highest PSNR on all ten test images, outperforming MBF, FNNM, AROMC, HOAT, and OSE. For example, on images G and E, IOSEBF improves over the next best method by 1.63 dB and 1.50 dB, respectively. Overall, the key advantage of IOSEBF lies in its robustness across diverse image textures, avoiding the dramatic fluctuations of HOAT and the consistently low PSNR values of MBF. These merits stem from two core design principles. First, IOSEBF reduces parameter redundancy: its subspace uses only r^2 parameters, far fewer than the n^2 parameters of OSE's self-expression matrix, and its dimensionality better matches the true rank, thus improving generalization. Second, the smooth surrogate admits closed-form solutions, avoiding slow convergence and reducing the need for manual parameter tuning. Consequently, IOSEBF not only

achieves the highest PSNR values but also provides a reliable and efficient solution for matrix completion.

For a visual comparison of the recovery results, Figure 6 shows some of the original images, incomplete images and the reconstructions given by IOSEBF and other methods.



Figure 6. The recovery results of IOSEBF and other compared methods. (E) The original image. (E1) The incomplete image. (E2) FNNM, PSNR = 33.87. (E3) HOAT, PSNR = 33.58. (E4) AROMC, PSNR = 33.45. (E5) MBF, PSNR = 32.26. (E6) OSE, PSNR = 34.67. (E7) IOSEBF, PSNR = 36.17.

Table 4. CPU times (in seconds) taken by IOSEBF and the other five methods to converge to the PSNR values listed in Table 3.

Image index	FNNM	AROMC	HOAT	MBF	OSE	IOSEBF
(A)	389.21	474.69	128.26	55.57	2180.28	**1.81**
(B)	376.59	2335.21	116.61	55.68	2148.89	**3.49**
(C)	391.29	2282.09	104.70	49.82	2124.21	**3.27**
(D)	386.47	2376.63	122.29	54.38	2237.29	**1.98**
(E)	375.99	2356.44	115.65	59.18	2018.95	**1.91**
(F)	399.25	2290.38	115.96	55.28	2207.84	**3.15**
(G)	385.64	2349.52	133.07	49.66	2109.58	**2.41**
(H)	377.22	2209.40	141.14	57.49	2200.77	**2.79**
(I)	359.36	2406.29	103.19	59.28	2100.16	**3.28**
(J)	388.37	2377.18	126.85	53.44	2174.33	**3.76**

As shown in Figure 6, the IOSEBF method produces a much clearer and visually more appealing recovery result compared to the other five methods, namely OSE, FNNM, HOAT, AROMC, and MBF. In particular, the reconstructed image given by HOAT in Figure 6(E3) contains many obvious noisy pixels scattered across the image, indicating that HOAT struggles to suppress noise effectively. For

FNNM and AROMC, whose results are shown in Figure 6(E2), (E4) respectively, the reconstructed images exhibit no obvious noise points; however, they appear relatively blurry overall, lacking sharpness in both edge regions and fine textures. The result of MBF in Figure 6(E5) not only has the lowest PSNR value among all methods, but also contains numerous small noise points and exhibits severely blurry edges, making it the least favorable reconstruction. In contrast, the reconstructed result of OSE in Figure 6(E6) achieves relatively clear edge details, which is a clear improvement over FNNM, AROMC, and MBF; nevertheless, it still retains many fine noise points, preventing it from reaching the high visual quality achieved by IOSEBF. Overall, IOSEBF stands out as the only method that simultaneously delivers high edge sharpness, low noise levels, and high PSNR values.

Finally, the CPU times of IOSEBF and the other compared methods are listed in Table 4, because the CPU time of IOSEBF is too small to be clearly visible if plotted in a figure.

As shown in Table 4, IOSEBF is by far the fastest among all six methods, requiring only about 2.8 seconds on average to converge to the highest PSNR values reported in Table 3. In comparison, MBF, which ranks second in speed, takes approximately 55 seconds, nearly 20 times longer than IOSEBF, yet its recovery quality is the poorest. HOAT and FNNM follow with average CPU times of about 121 and 383 seconds, respectively, both substantially slower than IOSEBF. More strikingly, OSE and AROMC, which achieve relatively high reconstruction accuracy, are extremely time-consuming, taking about 2150 and 2146 seconds on average, roughly 770 times longer than IOSEBF. Therefore, IOSEBF not only delivers the best PSNR performance but also outperforms all other methods by an overwhelming margin in computational efficiency. This unique combination of high accuracy and low time cost makes IOSEBF the most practical and attractive solution for large-scale matrix completion tasks.

5. Conclusions and future work

To improve the speed and accuracy of the OSE method, this paper proposes IOSEBF with bilinear factorization. By imposing the orthogonal subspace constraint on a small coefficient matrix, IOSEBF reduces the self-expression matrix from $n \times n$ to $r \times r$. On the one hand, the speed is improved by replacing large matrix inversion and eigenvalue decomposition with small $r \times r$ operations and by using QR decomposition and matrix multiplication instead of row-by-row reconstruction. On the other hand, the accuracy is improved by reducing parameter redundancy, which lowers the risk of overfitting and enhances generalization, and by avoiding the overfitting to local information caused by row-by-row reconstruction. Experiments on synthetic and real images show that IOSEBF achieves much higher accuracy than OSE and other methods, while being up to several hundred times faster.

Future work will focus on further improving IOSEBF. First, lower-complexity solvers will replace the eigenvalue decomposition and matrix inversion steps. Second, a fast rank-adaptive estimation scheme will be developed to avoid manual rank selection. Third, IOSEBF will be extended to structured and block missing patterns. Finally, a systematic comparison with deep-learning-based matrix completion methods will be conducted.

Use of AI tools declaration

No AI tool was used to generate any part of this paper.

Acknowledgments

This work was supported by the National Natural Science Foundation of China under Grant 62102002, by the Key Cultivation Project for Outstanding Young Teachers in Anhui Province China under Grant YQZD2024039, by the Research Start-up Fund of West Anhui University, No. WGKQ2021053 and by the Key Project of Scientific Research of Anhui Provincial Department of Education, No. 2025AHGXZK30493.

Conflict of interest

The authors declare that they have no known competing financial interests or personal relationships that could have appeared to influence the work reported in this paper.

References

1. Y. Wang, W. Li, J. E. Fowler, G. Vivone, Robust matrix completion with deterministic sampling via convex optimization, *IEEE Trans. Pattern Anal. Mach. Intell.*, **48** (2026), 6771–6785. https://doi.org/10.1109/TPAMI.2026.3659200
2. M. C. Tsakiris, Low-rank matrix completion theory via Plücker coordinates, *IEEE Trans. Pattern Anal. Mach. Intell.*, **45** (2023), 10084–10099. https://doi.org/10.1109/TPAMI.2023.3250325
3. X. Li, H. Zhang, R. Zhang, Matrix completion via non-convex relaxation and adaptive correlation learning, *IEEE Trans. Pattern Anal. Mach. Intell.*, **45** (2023), 1981–1991. https://doi.org/10.1109/TPAMI.2022.3157083
4. H. Cai, L. Huang, P. Li, D. Needell, Matrix completion with cross-concentrated sampling: Bridging uniform sampling and CUR sampling, *IEEE Trans. Pattern Anal. Mach. Intell.*, **45** (2023), 10100–10113. https://doi.org/10.1109/TPAMI.2023.3261185
5. Z. Y. Wang, X. P. Li, H. C. So, A. M. Zoubir, Adaptive rank-one matrix completion using sum of outer products, *IEEE Trans. Circuits Syst. Video Technol.*, **33** (2023), 4868–4880. https://doi.org/10.1109/TCSVT.2023.3250651
6. J. Miao, K. I. Kou, Color image recovery using low-rank quaternion matrix completion algorithm, *IEEE Trans. Image Process.*, **31** (2022), 190–201. https://doi.org/10.1109/TIP.2021.3128321
7. Q. Liu, Z. Lai, Z. Zhou, F. Kuang, Z. Jin, A truncated nuclear norm regularization method based on weighted residual error for matrix completion, *IEEE Trans. Image Process.*, **25** (2016), 316–330. https://doi.org/10.1109/TIP.2015.2503238
8. A. Eamaz, F. Yeganegi, M. Soltanalian, Matrix completion from one-bit dither samples, *IEEE Trans. Signal Process.*, **74** (2026), 1616–1630. https://doi.org/10.1109/TSP.2024.3445289
9. Y. Li, X. Sun, Euclidean distance matrix completion via asymmetric projected gradient descent, *IEEE Trans. Signal Process.*, **74** (2026), 355–371. https://doi.org/10.1109/TSP.2025.3650509
10. H. Shu, J. Li, Y. Jin, H. Wang, Guaranteed multidimensional time series prediction via deterministic tensor completion theory, *IEEE Trans. Signal Process.*, **73** (2025), 4638–4653. https://doi.org/10.1109/TSP.2025.3632844
11. Z. Wang, L. He, J. Miao, L. J. Deng, J. Liu, Low-rank reduced biquaternion matrix completion with application to color image inpainting, *Pattern Recognit.*, **180** (2026), 114021. https://doi.org/10.1016/j.patcog.2026.114021

12. X. Jin, J. Miao, Q. Wang, G. Geng, K. Huang, Sparse matrix factorization with L2,1 norm for matrix completion, *Pattern Recognit.*, **127** (2022), 108655. https://doi.org/10.1016/j.patcog.2022.108655
13. Z. Li, F. Nie, R. Wang, X. Li, Robust rank-one matrix completion with rank estimation, *Pattern Recognit.*, **142** (2023), 109637. https://doi.org/10.1016/j.patcog.2023.109637
14. R. Han, S. Liao, S. Fu, X. Wang, Transformed sparsity-boosted low-rank model for image inpainting with non-convex γ-norm regularization and non-local prior, *Opt. Laser Technol.*, **181** (2025), 111865. https://doi.org/10.1016/j.optlastec.2024.111865
15. K. Wang, B. Li, M. Xu, D. Ding, Q. Zheng, G. Tian, et al., MCLRP: Enhanced prediction of anticancer drug response through low-rank matrix completion and transcriptomic profiling, *BMC Biol.*, **24** (2026), 4. https://doi.org/10.1186/s12915-025-02457-8
16. H. Shu, H. Wang, J. Peng, D. Meng, Low-rank tensor completion with 3-D spatiotemporal transform for traffic data imputation, *IEEE Trans. Intell. Transp. Syst.*, **25** (2024), 18673–18687. https://doi.org/10.1109/TITS.2024.3422214
17. M. Fazel, *Matrix Rank Minimization with Applications*, Ph.D thesis, Stanford University, 2002. https://faculty.washington.edu/mfazel/thesis-final.pdf
18. J. Cai, E. Candès, Z. Shen, A singular value thresholding method for matrix completion, *SIAM J. Optim.*, **20** (2010), 1956–1982. https://doi.org/10.1137/080738970
19. K. C. Toh, S. Yun, An accelerated proximal gradient algorithm for nuclear norm regularized linear least squares problems, *Pacific J. Optim.*, **6** (2010), 615–640.
20. P. Jain, R. Meka, I. S. Dhillon, Guaranteed rank minimization via singular value projection, in *Advances in Neural Information Processing Systems 23 (NIPS 2010)*, (2010), 1–9.
21. Z. Wen, W. Yin, Y. Zhang, Solving a low-rank factorization model for matrix completion by a nonlinear successive over-relaxation, *Math. Program. Comput.*, **4** (2012), 333–361. https://doi.org/10.1007/s12532-012-0044-1
22. Y. Liu, L. Jiao, F. Shang, A fast tri-factorization method for low-rank matrix recovery and completion, *Pattern Recognit.*, **46** (2013), 163–173. https://doi.org/10.1016/j.patcog.2012.07.003
23. Y. Liu, L. Jiao, F. Shang, F. Yin, F. Liu, An efficient matrix bi-factorization alternative optimization method for low-rank matrix recovery and completion, *Neural Netw.*, **48** (2013), 8–18. https://doi.org/10.1016/j.neunet.2013.06.013
24. M. Yang, Y. Li, J. Wang, Feature and nuclear norm minimization for matrix completion, *IEEE Trans. Knowl. Data Eng.*, **34** (2022), 2190–2199. https://doi.org/10.1109/TKDE.2020.3005978
25. G. Chang, W. Zhang, L. Zhang, Matrix completion with incomplete side information via orthogonal complement projection, in *Proceedings of the 42nd International Conference on Machine Learning (ICML)*, (2025), 7393–7416.
26. A. Agarwal, J. Choi, M. Yuan, Robust matrix estimation with side information, preprint, arXiv:2603.24833.
27. H. Zhang, Z. Jiao, X. Li, Orthogonal subspace exploration for matrix completion, *Pattern Recognit.*, **153** (2024), 110456. https://doi.org/10.1016/j.patcog.2024.110456
28. W. Qu, X. Xiu, H. Chen, L. Kong, A survey on high-dimensional subspace clustering, *Mathematics*, **11** (2023), 436. https://doi.org/10.3390/math11020436
29. Z. Xing, W. Zhao, Clustering structure identification with ordering graph, *Knowl.-Based Syst.*, **343** (2026), 115999. https://doi.org/10.1016/j.knosys.2026.115999

30. Z. Xing, W. Zhao, Block-diagonal structure learning for subspace clustering, *Expert Syst. Appl.*, **285** (2025), 127767. https://doi.org/10.1016/j.eswa.2025.127767
31. Z. Xing, W. Zhao, Block-diagonal guided DBSCAN clustering, *IEEE Trans. Knowl. Data Eng.*, **36** (2024), 5709–5722. https://doi.org/10.1109/TKDE.2024.3401075
32. Y. H. Nazari, A. Tajaddini, F. S. Movahed, F. Alonso-Fernandez, P. Tiwari, Robust oblique projection and weighted NMF for hyperspectral unmixing, *Pattern Recognit.*, **170** (2026), 112029. https://doi.org/10.1016/j.patcog.2025.112029
33. Y. Yan, D. Cheng, J. E. Feng, H. Li, J. Yue, Survey on applications of algebraic state space theory of logical systems to finite state machines, *Sci. China Inf. Sci.*, **66** (2023), 111201. https://doi.org/10.1007/s11432-022-3538-4
34. Z. Wang, X. P. Li, H. C. So, Robust matrix completion based on factorization and truncated-quadratic loss function, *IEEE Trans. Circuits Syst. Video Technol.*, **33** (2023), 1521–1534. https://doi.org/10.1109/TCSVT.2022.3214583



AIMS Press

©2027 the Author(s), licensee AIMS Press. This is an open access article distributed under the terms of the Creative Commons Attribution License (http://creativecommons.org/licenses/by/4.0)